# A spatio-temporal analysis for detecting neural activation in the imaging data

Miwakeichi, Fumikazu
*The Institute of Statistical Mathematics, Department of Statistical Modeling*
*The Graduate University for Advanced Studies, Department of Statistical Science, School of Multidisciplinary Sciences,*
*10-3 Midori-cho, Tachikawa, Tokyo 190-8562, Japan*
*E-mail: miwake1@ ism.ac.jp*

Oku, Yoshitaka
*Hyogo College of Medicine, Department of Physiology*
*1-1 Mukogawa-cho, Nishinomiya, Hyogo 663-8501, Japan*
*E-mail: yoku@hyo-med.ac.jp*

Okada, Yasumasa
*Keio University, Department of Medicine, Tsukigase Rehabilitation Center*
*Tsukigase 380 2, Izu City, Shizuoka 410-3215, Japan*
*E-mail: yasumasaokada@1979.jukuin.keio.ac.jp*

Kawai, Shigeharu
*The Institute of Statistical Mathematics, Department of Statistical Modeling*
*10-3 Midori-cho, Tachikawa, Tokyo 190-8562, Japan*
*E-mail: s-kawai@zpost.plala.or.jp*

Tamura, Yoshiyasu
*The Institute of Statistical Mathematics, Department of Data Science*
*The Graduate University for Advanced Studies, Department of Statistical Science, School of Multidisciplinary Sciences,*
*10-3 Midori-cho, Tachikawa, Tokyo 190-8562, Japan*
*E-mail: tamura@ism.ac.jp*

Ishiguro, Makio
*The Institute of Statistical Mathematics, Department of Statistical Modeling*
*The Graduate University for Advanced Studies, Department of Statistical Science, School of Multidisciplinary Sciences,*
*10-3 Midori-cho, Tachikawa, Tokyo 190-8562, Japan*
*E-mail: ishiguro@ ism.ac.jp*

## I. INTRODUCTION

There have been many techniques to measure brain neural activities as spatio-temporal imaging data, e.g., functional magnetic resonance imaging (fMRI) and optical imaging. These techniques enable us to record spatio-temporal information of neural dynamics. A time series corresponds to each measurement point in spatial two or three-dimensional grid. In order to detect significant neural activities in large-scale spatio-temporal data, many statistical methods have been proposed. Among these methods, the methods in the framework of general liner model have been widely used in fMRI data analysis [1].

The structure of optical imaging data is three-dimensional, and two of them are for space and one is for time axes. Although the structure of optical imaging data is similar to that of fMRI data, there has been no widely used method for data analysis. Respecting to this situation, Oku *et al.* [2], [3] and Okada *et al.* [4] applied time-lagged correlation analysis to optical imaging data to elucidate the mechanism of respiratory rhythm and pattern generation in the rat and frog brainstem. They used 4th cervical spinal cord ventral root (C4VR) output signals that are equivalent to phrenic inspiratory burst activity as the reference function. However, there are several problems in these analyses. By the regression or correlation analysis, only the morphological resemblance between the time series and the reference function is evaluated. If there is some activation pattern that does not resemble the reference function, then it cannot be detected. More seriously, in the case that the reference function cannot be defined, the data can hardly be analyzed by these methods. Taking this problem into account, we proposed a fusion method comprising innovation approach in time series analysis and statistical test [5]. Autoregressive (AR) models were fitted to time series data of each pixel for the range sufficiently before or after the state transition. Then, the remaining time series data were filtered using these AR parameters to obtain its innovation (filter output). The proposed method could extract brain neural activation as a phase transition of dynamics in the system without employing external information such as the reference function. The activation could be detected as temporal transitions of statistical test values. In the previous study, we analyzed repeatedly recorded optical imaging data to increase the number of samples for the evaluation of amplitude level of innovations. The evoked neural responses to some stimulus or those accompanied by cyclic neural activity, such as respiration, can be detected by repeated recording with multiple trials and averaging, because our proposed method in the previous study cannot be directly employed to evaluate specific activity in a single trial. Therefore, the changing of neural activity among trials could not be evaluated. In the current study, we introduce a method for analyzing single trial data by modifying the previously proposed method.

## II. METHODS

The autoregressive (AR) model for a time series $\eta(t), t=1,\ldots,S,$ is defined as a linear combination of the past values with a prediction error $\varepsilon(t)$ and a constant $\beta$,

$$\eta(t)-\beta=\sum_{i=1}^{p}\alpha(i)\eta(t-i)+\varepsilon(t) \tag{1}$$

where $p$ denotes the model order and $\alpha(i)$ are AR coefficients. The linear dynamic properties of the system can be identified with a parameter vector $\boldsymbol{\vartheta}=\{\alpha(1),\ldots,\alpha(p),\beta,\sigma_\varepsilon^2\}$, here $\sigma_\varepsilon^2$ is a variance of $\varepsilon(t)$. The

innovations resulting from the residual time series can be estimated as

$$\varepsilon(t)=\eta(t)-\hat{\eta}(t)=\eta(t)-\left(\sum_{i=1}^{p}\alpha(i)\eta(t-i)+\beta\right) \tag{2}$$

and the signals that cannot be predicted by the linear AR process remain in the innovations. In other words, innovations are filter outputs through a linear AR process.

Considering an exogenous input $\gamma(t),\ t=1,\ldots,S,$ the AR model can be generalized to an AR model with exogenous inputs (ARX) denoted as

$$\eta(t)-\beta=\sum_{i=1}^{p}\alpha(i)\eta(t-i)+\sum_{j=1}^{q}\phi(j)\gamma(t-j)+\varepsilon(t) \tag{3}$$

Suppose the measurement points of the imaging data are on the two dimensional pixels that are labeled by an index $v=(l,m)$ and only the influences of nearest neighbor upon each pixel are considered as exogenous inputs, the ARX model will be specialized as

$$\begin{aligned}&\eta^{v}(t)-\beta^{v}\\&=\sum_{i=1}^{p}\alpha^{v}(i)\eta^{v}(t-i)+\sum_{\boldsymbol{u}\in \mathrm{N}(\boldsymbol{v})}\sum_{j=1}^{q}\delta^{\boldsymbol{u}}(j)\eta^{\boldsymbol{u}}(t-j)+\varepsilon^{v}(t),\end{aligned} \tag{4}$$

where $\mathrm{N}(\boldsymbol{v})$ is a set of indices of the neighbor pixels for the pixel at $v=(l,m)$. Suppose neighbor pixels are restricted to the pixels, which contact with the edge of the pixel at the point $v$, a set of indices of neighbor pixels will be

$$\mathrm{N}(\boldsymbol{v})=\left\{(l+1,m),(l,m-1),(l,m+1),(l-1,m)\right\}. \tag{5}$$

The ARX model with the restricted neighbor pixels will be referred as Nearest Neighbor Autoregressive model (NNAR) in this paper. The innovations for the pixel at $v$,

$$\begin{aligned}&\varepsilon(t)^{v}=\eta^{v}(t)-\hat{\eta}^{v}(t)\\&=\eta^{v}(t)\\&\quad-\left(\sum_{i=1}^{p}\alpha^{v}(i)\eta^{v}(t-i)+\sum_{\boldsymbol{u}\in \mathrm{N}(\boldsymbol{v})}\sum_{j=1}^{q}\delta^{\boldsymbol{u}}(j)\eta^{\boldsymbol{u}}(t-j)+\beta^{v}\right)\end{aligned} \tag{6}$$

contain the signals which would not be predicted by a linear AR process even if the spatial influences from the neighbors were taken into consideration.

Suppose the NNAR model is identified with a limited period $t_1\le t\le t_2$, any arbitrarily selected other period $t_1'\le t\le t_2'$ can be filtered through the identified NNAR model. Let the innovations corresponding to the period for the NNAR model identification and for filtering $\varepsilon^{1,v}(t)$ and $\varepsilon^{2,v}(t)$ respectively. The amplitude level of $\varepsilon^{2,v}(t')$ will increase at the time point $t'$ when the unpredictable signals arise. In order to evaluate the amplitude level, we compared the mean values between the innovations in the time window $t'-(w/2)\le t'\le t'+(w/2)$ (the window width is $w+1$, $w$: even integer ), $\left(1/(w+1)\right)\sum_{n=t'-(w/2)}^{t'+(w/2)}\varepsilon^{2,v}(t')$ and whole innovations within the period $t_1\le t\le t_2$, $(t_2-t_1+1)^{-1}\sum_{t=t_1}^{t_2}\varepsilon^{1,v}(t)$ by some statistical test. In this study, we employed standard *t*-test for this purpose. By shifting time point $t'$, time-dependent *t*-values can be computed. Then time-dependent activation *t*-map, which shows dynamic state transition, can be obtained by repeating

this procedure for all pixels.

## III. DATA ACQUISITION

Fig.1 shows the recorded area in the brainstem of neonatal rat, which contains two putative respiratory rhythm generators, the para-facial respiratory group (pFRG) and the pre-Bötzinger complex (preBötC). Inspiratory-related respiratory activity was monitored from the C4 ventral root (C4VR) with a suction electrode. The raw nerve signal was amplified, band-pass filtered from 15 Hz to 3 kHz, full-wave rectified, and integrated with a decay time constant of 100ms. The recording chamber was mounted on a fluorescence macro zoom microscope (MVX-10, Olympus Optical, Tokyo, Japan). Preparations stained with a voltage-sensitive dye (di-2-ANEPEQ, Invitrogen, Carlsbad, CA, USA) were illuminated with a tungsten–halogen lamp (150W) through a band-pass excitation filter ($\lambda$=480–550 nm). Epifluorescence through a long-pass barrier filter ($\lambda$>590 nm) was detected with a CMOS sensor array (MiCAM Ultima L-camera, BrainVision; 100 $\mu$m×100 $\mu$m pixel size, 100×100 pixel array). Optical signals were sampled at 50 Hz (20 ms/frame). Analog signals of raw and integrated C4VR activities were recorded at 1 kHz. These analog signals were digitized, and stored in a hard disk together with optical signals. Analog signals were window-discriminated to yield Transistor-Transistor Logic (TTL) pulses and used to trigger the optical recording system. Total number of recorded time frames were 1024, the recording was started at 768 frames before the trigger signal, and repeated 30 times. Among these trials, 29 trials, which were contaminated with relatively small artifacts, were selected.

The change in fluorescence intensity ($\Delta F$) relative to the initial intensity of the fluorescence ($F_0$) in each pixel was calculated. To normalize the difference in the amount of membrane-bound dye and illumination within the preparation, background fluorescence intensity at each pixel was divided by the maximum background fluorescence, and then the ratio of $\Delta F$ to the normalized background fluorescence intensity (F), i.e., the fractional change in fluorescence intensity ($\Delta F/F$), was calculated at each pixel in each frame. If F was less than 0.25, then $\Delta F/F$ was set to be zero. Then the linear trend of imaging data associated with photobleaching was eliminated and z-transformed.

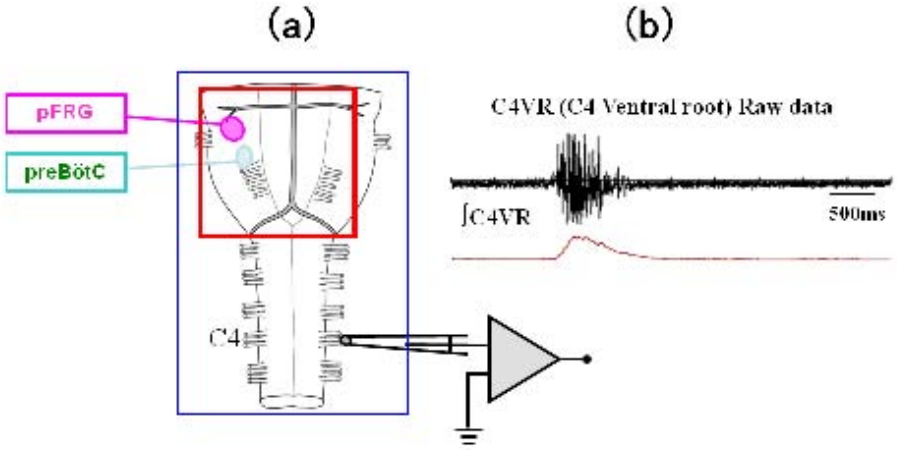


Fig.1

(a) Schematic representation of anatomical structure of the brainstem and the recorded area, (b) Raw output signal from C4VR (upper) and Integrated C4VR output signal (lower).

## IV. RESULTS

Background stationary oscillations were identified by a NNAR model on the period sufficiently before the onset of inspiratory activity. In this study four neighboring pixels, which contact with edges of a pixel of interest were employed for the NNAR model to save the computational cost. The parameters in the NNAR model were estimated using the least square method. Then the rest part of the data was filtered through the identified model and the innovations were estimated. We defined the origin of time axis as the onset of inspiratory activity observed in the C4VR signal. The NNAR model was identified on the period sufficiently before the onset of inspiratory activity, i.e., from -4.22s to -2.24s (100 time frames). Subsequently, the period from -2.22s to 5.24s (374 time frames) was filtered. The model order for $p$ and $q$ in (6) was selected to $p = q = 7$ by the same procedure in the previous study [5]. And the window width was adjusted to $w + 1 = 31$. We repeated the analytical procedure explained in the section "II. METHODS" for all trials.

In order to investigate the basic oscillatory properties of the data, we computed power spectrum using standard Fast Fourier Transformation (FFT). Fig.2(c) shows averaged power spectrum across all pixels and all trials of imaging data and innovations. There were three major peaks in the power spectrum of the imaging data, which corresponded to about 0.1-0.5Hz, 3.0-6.0Hz and 12.0-14.0Hz, respectively. Spatial distribution maps corresponding to these peaks are represented in Fig.2(a) and (b) for the raw data and innovations, respectively. A pixel group with higher intensity (located in the red circle) on the spatial distribution map for 0.1-0.5 Hz nearly corresponded to the respiratory-related regions. On the other hand, the latter two would correspond to stationary background signals originating from mechanical oscillations of the recording system and/or turbulence associated with circulation of the perfusion fluid. The peaks corresponding to these background oscillations significantly diminished in the power spectrum of innovations (Fig.2(b)). Moreover, the spatial distribution maps of power were nearly homogenous, and any characteristic structure could not be observed, suggesting that the background stationary oscillations were accurately identified by the NNAR model and removed from the innovations. Because of the difference in the amplitude of imaging data and innovations, the intensity of power spectrum cannot be directly compared (the amplitude of innovations are smaller than imaging data). Therefore, the power spectrums were normalized.

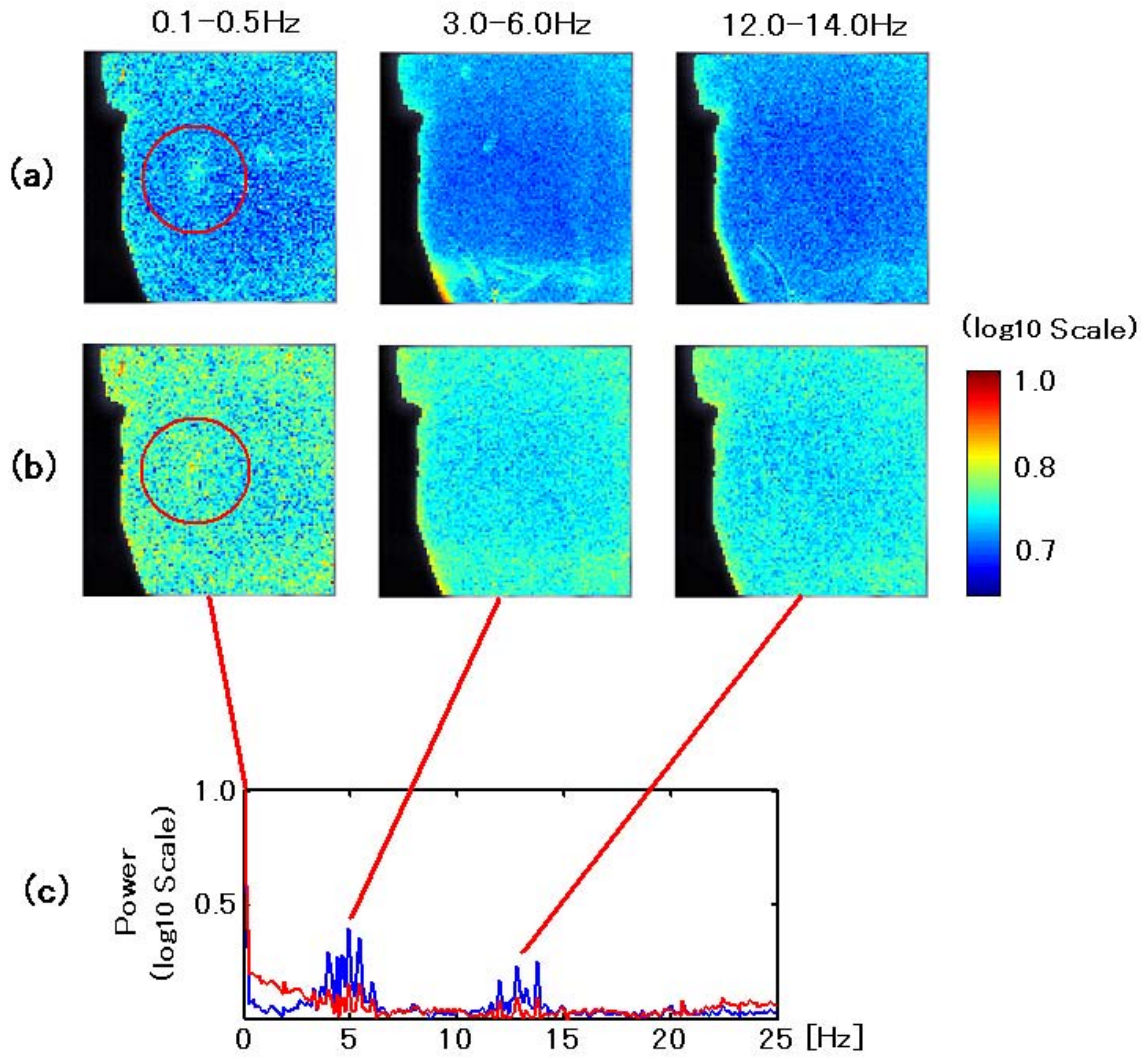


Fig.2

Spatial distribution of averaged power spectrum in a specific frequency band for the optical recording data (a) and innovations (b). (c) Normalized averaged spectral power across all pixels and all repetitions for the optical recording data (blue line) and innovations (red line). The red circle indicates the region where respiratory-related neuron group locates.

The amplitude of the innovation in the period of filter output will increase when unpredictable signal by the identified NNAR model appears. Then we evaluated the statistical significance of the difference of mean amplitude of the innovations using standard *t*-test. This procedure was repeated for all pixels, and then temporal transition of activation *t*-map was illustrated. Five representative time frames of activation time map are illustrated as time dependent *t*-maps in Fig.3(b), which shows the area and time at which significant dynamic state transition arises. The activation initiated at the caudal part of pFRG, corresponding to the rostral ventrolateral medulla (RVLM) [6] and [7], and then extended rostrally toward the rostral part of pFRG and caudally toward the preBötC. Fig.3(a) displays activation *t*-maps for the raw imaging data instead of the innovations using the procedure described above. Although both images for the imaging data and innovations were thresholded at the same level, significant areas for the imaging data were less than those for the

innovations.

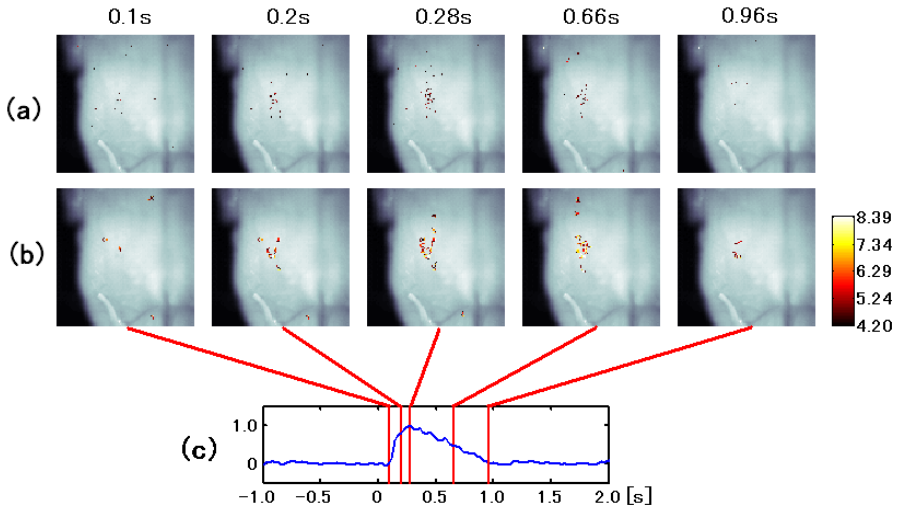


Fig.3

Representative time frames of temporal transition of the activation *t*–maps for the imaging data (a) and the innovations (b). The C4VR output signal and time points corresponding to the time frames (c). The *t*-maps were thresholded with $p<0.05$ (corrected by the False Discovery Rate (FDR)) and a cluster extent of five pixels.

## V. DISCUSION

In the previous study, we evaluated the amplitude of innovations across all trials. It was necessary to use multiple trials and averaging to overcome a low S/N ratio of the data. Alternatively, in the present study, we attempted to detect neuronal activities within a single trial using a sliding window instead of multiple trials. In both cases, two measure respiratory-related regions, pFRG and preBötC, could be successfully detected. However, in the case of a single trial, the activation in the caudal brainstem area (in regions caudal to the preBötC) could not be found. The activations of pFRG and preBötC could be detected about 40% of trials. We also analyzed another data set comprising 256 time frames. In this case, any respiratory-related regions could not be detected, suggesting that the investigation time frames should be carefully chosen based on the quality of data.

We conclude that our method is capable of detecting neuronal activation within a single trial. This method can be widely employed for the analysis of the changing of neural activity among trials and the data set from other spontaneous neural activities, such as EEG spindle waves, epileptic waves and so on.

**References**

[1] K. J. Friston, A. P. Holmes, K. J. Worsley, J. B. Poline, C. D. Frith, and R. S. J. Frackowiak, "Statistical parametric maps in functional imaging: A general linear approach," *Hum. Brain. Mapp.*, vol.2, no. 4, pp. 189-210, 1995.

[2] Y. Oku, H. Masumiya, and Y. Okada, "Postnatal developmental changes in activation profiles of the respiratory neuronal network in the rat ventral medulla," *J. Physiol.*, vol. 585, no. 1, pp. 175-186, 2007.

[3] Y. Oku, N. Kimura, H. Masumiya, and Y. Okada, "Spatiotemporal organization of frog respiratory neurons visualized on the ventral medullary surface," *Respir. Physiol. Neurobiol.*, vol. 161, no. 3, pp. 281-290, 2008.

[4] Y. Okada, H. Masumiya, Y. Tamura, and Y. Oku, "Respiratory and metabolic acidosis differentially affect the respiratory neuronal network in the ventral medulla of neonatal rats," *Eur. J. Neurosci.*, vol. 26, no. 10, pp. 2834-2843, 2007.

[5] F. Miwakeichi, Y. Oku, Y. Okada, S. Kawai, Y. Tamura and M. Ishiguro,"Detection and visualization method of dynamic state transition for biological spatio-temporal imaging data", IEEE Transaction on Medical Imaging, vol.30, no. 3, pp. 859-66, 2011

[6] H. Onimaru, and I. Homma I, "A novel functional neuron group for respiratory rhythm generation in the ventral medulla", *J. Neurosci.*, vol. 23, no. 4, pp.1478-1486, 2003.

[7] H. Onimaru, A. Arata, and Homma I, "Primary respiratory rhythm generator in the medulla of brainstem-spinal cord preparation from newborn rat", *Brain Res.*, vol. 445, no.2, pp.314-324, 1988.